Plasma-functionalized multi-walled carbon nanotubes directly grown on stainless steel meshes as supercapacitor electrodes

OPEN ACCESS
IOP Publishing
Journal of Physics D: Applied Physics
J. Phys. D: Appl. Phys. **55** (2022) 194001 (12pp)
https://doi.org/10.1088/1361-6463/ac4fd8

Plasma-functionalized multi-walled carbon nanotubes directly grown on stainless steel meshes as supercapacitor electrodes

Elmira Pajootan[1,2,*], Minnan Ye[2], Muyang Zhang[2], Sogol Niroumandrad[2], Sasha Omanovic[2] and Sylvain Coulombe[1]

[1] Catalytic and Plasma Process Engineering, McGill University, 3610 University Street, Montréal, Québec H3A 0C5, Canada
[2] Electrochemistry/Corrosion Laboratory, Department of Chemical Engineering, McGill University, 3610 University Street, Montréal, Québec H3A 0C5, Canada

E-mail: elmira.pajootan@mail.mcgill.ca

Received 17 November 2021, revised 24 January 2022
Accepted for publication 28 January 2022
Published 11 February 2022

Abstract

Multi-walled carbon nanotubes (MWCNTs) directly grown on a stainless steel mesh were functionalized using a fast, solvent-free radiofrequency (RF) plasma technique. Two different gas mixtures of $Ar/C_2H_6/O_2$ and $Ar/C_2H_6/N_2$ were used to add oxygen- and nitrogen-containing functional groups to the surface of MWCNTs. The binder-free forest-like MWCNTs before and after functionalization were tested as supercapacitor electrodes. The structural and electrochemical characteristics of the electrodes were evaluated. The RF power (10–30 W) and functionalization time (1–20 min) were optimized to achieve the highest capacitance. Both nitrogen- and oxygen-functionalized MWCNTs showed improved capacitive behavior due to the presence of the functional groups on the MWCNT surface. The highest capacitance was obtained for the MWCNT electrode functionalized with the RF plasma employing the $Ar/C_2H_6/O_2$ gas mixture at 20 W for 15 min, reaching the specific capacitance of 37.3 ± 1.1 mF cm^{-2} (196.3 ± 5.8 F g^{-1}).

Supplementary material for this article is available online

Keywords: radiofrequency plasma, multi-walled carbon nanotubes, solvent-free functionalization, supercapacitors

(Some figures may appear in color only in the online journal)

1. Introduction

The urgency to transition away from fossil fuels drives new renewable energy production, conversion and storage developments with high efficiency, affordability and sustainability characteristics. Electrochemical capacitors (or supercapacitors (SCs)) and batteries are crucial in advancing energy storage devices for many applications, such as hybrid electric vehicles, portable medical electronics and military devices. Because of their high energy density, batteries are widely used in automobile applications. However, the drawbacks of batteries stem from their working principles; low power density, lengthy recharge, progressive degradation and high replacement costs. Compared to batteries, SCs have higher power density, extended cycle stability and faster charge–discharge characteristics

* Author to whom any correspondence should be addressed.

and thus, are one of the promising solutions to current energy storage requirements. Consequently, electrochemical SCs are particularly useful for high power bursts, such as accelerating and breaking of high-speed transportation systems. However, SCs suffer from lower energy density compared to batteries [1–5].

To overcome the low energy density of SCs, carbonaceous materials, especially carbon nanotubes (CNTs) providing a high surface to volume (or mass) ratio, superior electrical conductivity, global abundance, low cost and high stability in severe environments, have become one of the most extensively studied nanomaterials contributing to the growing energy storage applications, more specifically in flexible electrode fabrication. Flexible SCs are in high demand for portable electronic devices, which require a flexible, lightweight, and mechanically robust substrate. However, most carbon materials are in powder or flake form; thus, electrode fabrication requires binders in contact with the current collector. The non-conductive nature of the binders results in a higher resistance, reducing the capacitance by covering (insulating) the active surface of the electrode material [6–8]. In addition, the relatively poor contact between the active electrode material (carbon powder) and the current collector contributes to an increased equivalent-series-resistance in the SC, lowering the total power and energy density.

A binder-free growth of CNTs is enabled by using inexpensive stainless steel (SS) mesh material as a flexible support (current collector), allowing the entire surface of the nanotubes to be accessible with low electrical contact resistance [9, 10]. However, CNTs store charge via electrochemical double-layer capacitance, and their hydrophobic nature hinders their interaction (contact area) with the aqueous electrolyte, resulting in a low power/energy density. To overcome this issue and increase their surface hydrophilicity, surface modification or functionalization to add hydrophilic functional groups or deposit metal oxides can be performed. Furthermore, functionalizing CNTs allows charge storage through the pseudo-capacitive mechanism via the reversible surface redox reactions, thus increasing the overall capacitance of the electrode [6, 11, 12]. Several techniques have been used to modify the surface of CNTs, including covalent functionalization, e.g. using chemical modification with carboxylic groups by refluxing the CNTs in strong acid solutions [13]. Another method is the non-covalent functionalization using adsorption forces, such as hydrogen bonding and electrostatic, by adsorbing amine-functionalized dendrimer molecules [14]. Functionalization with polymers, biomolecules, surfactants, decoration with nanoparticles, and plasma functionalization are other techniques used to modify the surface of CNTs [15].

Plasma technologies are gaining more attention for many applications, especially in energy conversion and environmental fields [16, 17]. Since processing plasmas contain various reactive species such as electrons, ions, atoms, and molecules, the plasma can effectively alter the chemical surface properties of carbon materials by forming active species on the surface [18]. The plasma treatment can be dry and solvent-free, thus reducing the environmental footprint. It features fast turn-on and turn-down times, short reaction times, and can be performed at low to moderate temperatures. Extensive tunability of the plasma chemistry and types of functional groups grafted on exposed surfaces can be achieved by changing the plasma conditions (i.e. gas type and pressure, power and duration of treatment) [19–22].

In this work, multi-walled CNTs (MWCNTs) with a forest-like structure were directly grown on a SS mesh (current collector) via a binder-free and catalyst-free chemical vapor deposition (CVD) technique. This approach leads to a low contact electrical resistance and no agglomeration of the nanotubes, two important properties for SC electrodes. The MWCNTs were further treated with a radio-frequency (RF) plasma using two gas mixtures of $Ar/C_2H_6/O_2$ and $Ar/C_2H_6/N_2$ to add oxygen- and nitrogen-containing functional groups on their surface. The functionalized and non-functionalized MWCNTs were characterized by transmission electron microscopy (TEM), scanning electron microscopy (SEM), scanning transmission electron microscopy (STEM), energy dispersive x-ray spectroscopy (EDS), x-ray photoelectron spectroscopy (XPS), Raman spectroscopy, and thermal gravimetric analysis (TGA). The capacitance of the MWCNTs before and after plasma functionalization was evaluated using cyclic voltammetry (CV), galvanostatic charge–discharge (GCD), and electrochemical impedance spectroscopy (EIS). Through this study, we aim to demonstrate that the capacitance behavior of porous, agglomeration-free functionalized MWCNT/SS electrodes is improved due to the increased hydrophilicity and additional charge storage through the pseudo-capacitive mechanism.

2. Materials and methods

2.1. Growth and functionalization of MWCNTs

MWCNTs were synthesized by thermal CVD in a quartz tube furnace using acetylene gas (MEGS, dissolved) as the carbon source and a SS mesh (SS316L, grid bars: 165 $\times$ 800 per 6.45 cm^2; thickness: 0.150 mm; wire diameters: 0.07 and 0.05 mm; grid opening: 15 μm, TWP Inc.) as the support for direct growth. The surface of the mesh was oxidized in the CVD furnace by exposure to air for 2 min; then the furnace was purged with Ar (Praxair, 99.999% purity) for 5 min to remove O_2 from the furnace. The growth of MWCNTs started by feeding C_2H_2 (68 $\pm$ 5 sccm) and Ar (592 $\pm$ 5 sccm) to the furnace for 2 min. To complete the growth, the C_2H_2 flow was stopped, and Ar was allowed to flow for another 2 min. Finally, the MWCNT-covered mesh was cooled down to room temperature [9, 10]. This synthesis process leads to the growth of a dense forest of intertwined MWCNTs on the SS, thus forming a porous electrode with high specific surface area.

The functionalization step was performed using a continuous wave low-pressure capacitively-coupled RF plasma (13.56 MHz). Prior to functionalization, Ar was injected into the vacuum chamber for 3 min and then pumped down to 10^{-5} Torr to reduce the air/moisture content. During functionalization, the chamber pressure was maintained at 2 Torr by continuously flowing a gas mixture of Ar (Praxair, 99.999% purity), C_2H_6 (MEGS, 99.995%), with O_2 (MEGS, 99.993%

purity) or N_2 (MEGS, 99.999% purity) at the flow rates of 250, 1 and 5 sccm, respectively, to functionalize the MWCNTs with oxygen (O-FMWCNT) or nitrogen (N-FMWCNT) functional groups. Ar is used as the main plasma forming gas to ensure the stability and treatment uniformity. Ethane (C_2H_6) was added as a source of carbon and hydrogen in the gas mixture, allowing the formation of oxygen- and nitrogen-rich plasma polymers [23]. The sample was placed on a live SS disk electrode (6 cm diameter) and the ground electrode was a SS disk of 10 cm placed 3 cm away. The RF plasma power levels and treatment times were 10, 20 and 30 W and 1, 2.5, 5, 10, 15 and 20 min, respectively. At the end of the experiment, the chamber was pressurized by injecting Ar until atmospheric pressure was reached.

2.2. Structural characterization

The structure of the MWCNT forest on SS was investigated by high-resolution field emission SEM, STEM (Hitachi, Cold FE SU-8000 SEM/STEM), and TEM (Thermo-Scientific, Talos F200X G2 TEM). EDS (XMax 80 mm^2 Oxford Instruments) was used under STEM mode for elemental mapping of the samples. For TEM imaging, the porous electrode was sonicated for 1 min in acetone (Sigma-Aldrich) to break off individual nanotubes from the SS mesh and collect them on a TEM Cu-grid. XPS (Thermo-Scientific, K-Alpha XPS apparatus, Al Kα source, micro-focused monochromator and spot size of 200 μm) was utilized to study the elemental composition and chemical state of the carbon structure before and after functionalization. The flood gun was used during the measurement to avoid substrate charging, and data analysis was performed by the Avantage software (Thermo Fisher Scientific). Raman spectroscopy (Thermo-Scientific, DRX2, laser excitation wavelength of 532 nm) was carried out to assess the structural integrity of the MWCNTs before and after functionalization. TGA (TA Q500, TA Instruments, USA) was performed over a temperature range of 20 °C–800 °C under air at a constant heating rate of 50 °C min^{-1} to determine the mass of MWCNTs grown on the SS from the mass loss. Optical emission spectroscopy (OES) was used to qualitatively detect the main species present in the plasma. The tip of an optical fiber was placed directly in front of the vacuum chamber glass viewport and the other end connected to a portable spectrometer (Ocean Optics USB2000) to record the spectra in the 200–1000 nm range with the spectral resolution of 1 nm.

2.3. Electrochemical tests

The electrochemical performance of all samples was assessed by CV, GCD and EIS, in a 4 M KOH solution (90% assay, Sigma-Aldrich, Germany) using a three-electrode cell with Hg/HgO reference electrode, platinum wire counter electrode, and MWCNTs/SS working electrode. The geometric surface area of the working electrode exposed to the electrolyte was 0.785 cm^2. Prior to all experiments, the electrolyte was purged with Ar for 40 min to remove the oxygen dissolved in the electrolyte. In order to obtain reproducible electrode surface behavior, the working electrode was cycled 70 times in the potential range of −0.7–0.3 V at a scan rate of 100 mV s^{-1} in Ar-saturated 4 M KOH before each experiment. To determine the capacitance, CV was performed in the same potential window at different scan rates, and GCD was carried out at different current densities. The specific capacitance from these tests was respectively calculated using equations (1) and (2) [24, 25]:

$$C_s = \frac{1}{m \times r \cdot (V_f - V_i)} \int_{V_i}^{V_f} I(V)\,dV = \frac{Q}{2 \times m \times (V_f - V_i)} \quad (1)$$

$$C_s = \frac{I \times \Delta t}{(V_f - V_i) \cdot m} \quad (2)$$

where C_s is the specific capacitance in F g^{-1}, m is the mass of MWCNTs per unit geometric area in g cm^{-2}, r is the scan rate in V s^{-1}, $\int_{V_i}^{V_f} I(V)\,dV$ is the area under cyclic voltammograms within the potential window representing the charge, Q is the total electric charge in Coulombs, Δt is the charge/discharge time in seconds, I is the applied current in Amperes and $V_f - V_i$ is the potential window.

All electrochemical tests were repeated three times, and the average and standard deviation values are reported. EIS measurements were conducted by applying a sinusoidal potential of 10 mV (peak) at a *dc* working electrode potential of −0.2 V in a frequency range from 100 kHz to 10 mHz. The NOVA 2.1.5 software was used for modeling the Nyquist plots with an equivalent circuit.

3. Results and discussions

3.1. MWCNT growth

Figures 1(a–a″) and (b–b″) shows SEM images of the SS mesh before and after the pre-treatment oxidation step. It should be explained that the growth temperature of MWCNTs on SS was first optimized, and the corresponding explanation is provided in the supporting information (S.1. Optimization of MWCNT growth temperature available online at stacks.iop.org/JPhysD/55/194001/mmedia). As shown in figure 1(b–b″), the surface of SS becomes rougher after the oxidation step. According to the SEM and TEM images in figures 1(c–c″) and (d–d″), at 700 °C, multi-walled and bamboo-like CNTs predominantly grew on the surface of the SS (diameter: ∼30–40 nm and length: ∼13–15 μm). Furthermore, different types of defects such as wall stacking faults, kinks and encapsulated fullerenes were observed in the TEM images. These are high-energy sites suitable for binding functional groups. The d-spacing of 0.35 nm marked in figure 1(c″) is attributed to MWCNTs [9].

The XPS survey scans in figure 1(e) identified Fe, Mn, Cr, C and O on the surface of SS, while after the oxidation step, Ni was also detected during the surface analysis. The surface percentage of Fe increased significantly from 12 to 30 at% during the SS oxidation, providing accessible catalyst on the surface

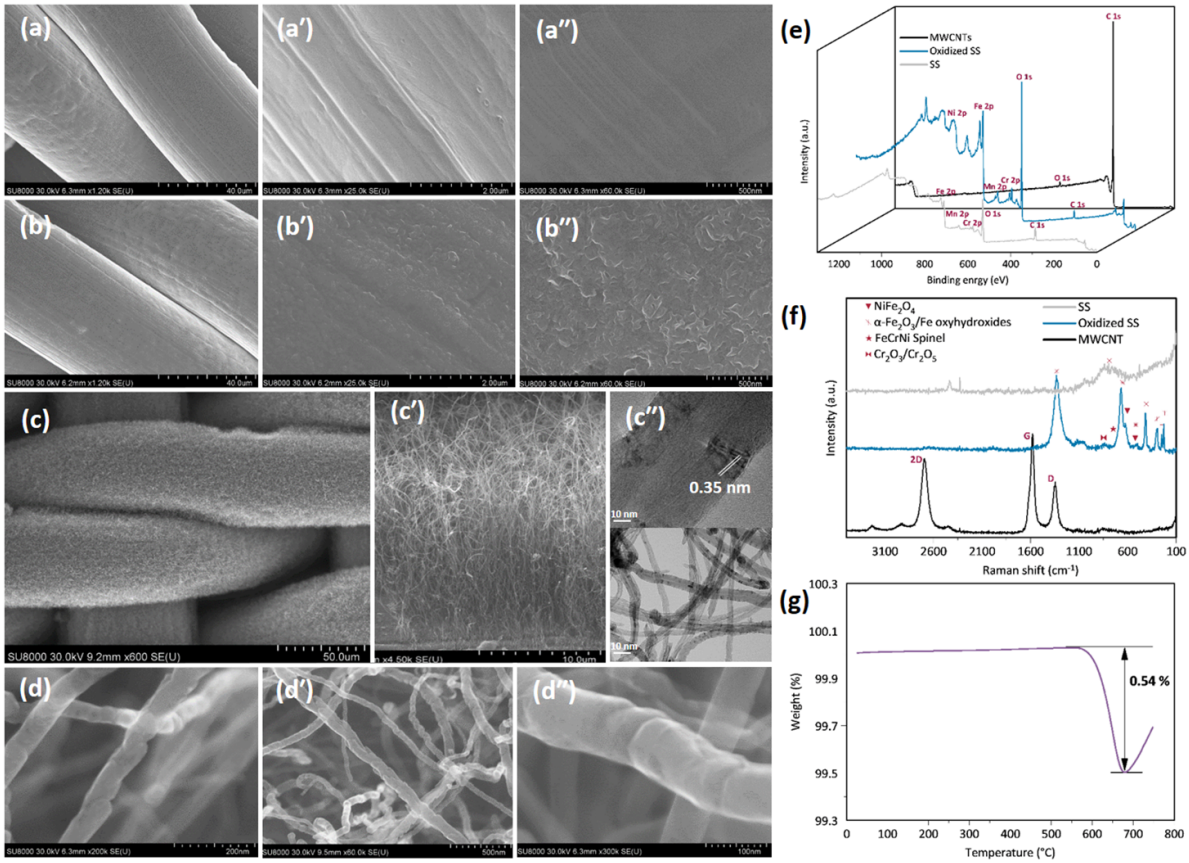

Figure 1. SEM images of (a–a″) SS, (b–b″) oxidized SS, and (c–c′) MWCNTs grown at 700 °C on SS. (c″) and (d–d″) are TEM images of MWCNTs on SS. (e) XPS survey scans, (f) Raman spectra of SS, oxidized SS and MWCNT/SS, and (g) TGA of MWCNT/SS.

of SS for the direct growth of MWCNTs. After the growth of MWCNTs on SS, the XPS survey scan indicated 98% of C and only 2% of O as the main elements, proving that a forest of metal-free MWCNTs is grown on SS.

Moreover, the Raman spectra displayed in figure 1(f) confirm the existence of oxide species on the surface of the oxidized SS with peaks at 1324, 850, 657, 612, 417, 293, 247 and 224 cm^{-1}, whereas for MWCNTs, the vibrational modes of nanotubes (D, G and 2D bands) are detected, which are further explained in the supporting information (section S.1.) [26, 27]. Figure 1(g) displays the average mass loss result of MWCNT/SS during TGA. No mass loss related to amorphous carbon is evident at temperatures below 450 °C, while the mass loss of 0.54 wt% at temperatures higher than 540 °C is due to the loss of graphitized carbon (MWCNTs) [9, 28]. Therefore, an area mass density of 0.19 ± 0.02 mg_{MWCNT} $cm^{-2}{}_{SS}$ was used to calculate the specific capacitance of the electrodes.

3.2. MWCNT plasma functionalization

The as-grown MWCNTs were functionalized with nitrogen- and oxygen-containing plasma gas mixtures at RF power levels of 10, 20 and 30 W for 1, 2.5, 5, 10, 15 and 20 min. The optical emission spectra recorded during the RF functionalization step are presented in figures S3(a) and (b). The hydroxyl radical molecular emission band, argon and oxygen peaks, and the first and second positive band systems of N_2 are recognizable. No significant carbon species emission is observed. The overall forest-like structure of MWCNTs on SS was not affected by the plasma functionalization at moderate power levels, and no observable degradation or damage to individual nanotubes was evident. Figure 2(a) shows the selected XPS spectra of C 1s of the as-grown MWCNTs before and after plasma functionalization using the $Ar/C_2H_6/O_2$ gas mixture.

The C 1s peaks were deconvoluted using the Avantage software to investigate the degree of functionalization of MWCNTs. As figure 2(a) shows, the high-energy side of the C 1s peak broadened after functionalization, confirming the presence of oxygen-containing functional groups on the surface of MWCNTs. The C 1s peaks were fitted using six components. The three main carbon components are the asymmetric graphene sp^2 component at 284.45 eV, symmetric sp^3 carbon at 284.9 eV and π-plasmon at 290.5 eV. The functional groups from low (285.5 eV) to high (288.5 eV) binding energies can be C−N, C−O or C−O−N, C=O or C=N, and C=O−O or N=C−O [23, 29, 30]. Furthermore, a thin layer of amorphous carbon was observed by TEM imaging of the surface of a nanotube, shown in figure 2(b). This amorphous structure forms due to the existence of C_2H_6 in the gas mixture, resulting in the formation of a plasma polymer film

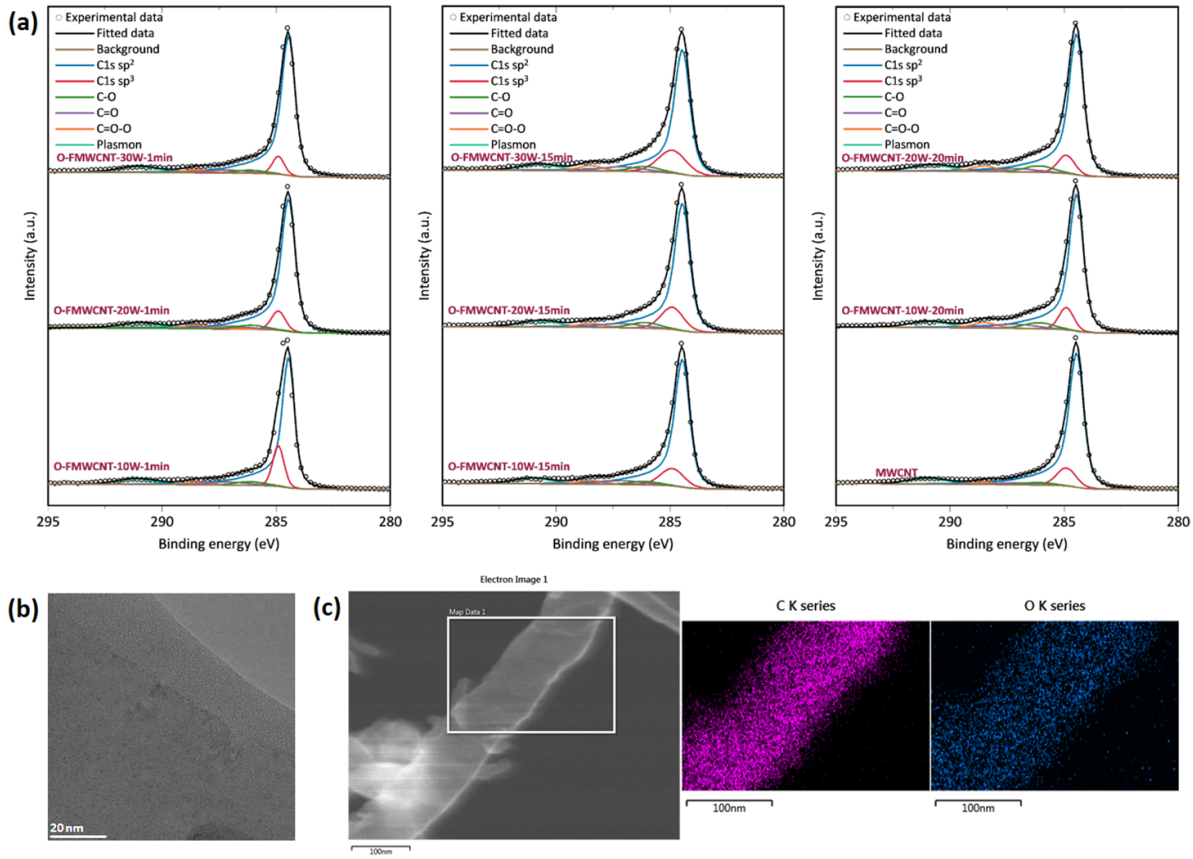

Figure 2. (a) Deconvoluded XPS spectra of C 1s for O-FMWCNT samples. (b) TEM image, and (c) STEM image and EDS mapping of O-FMWCNT-20 W–15 min.

on the MWCNTs. Additionally, the STEM imaging and EDS mapping of O-FMWCNT functionalized at 20 W for 15 min in figure 2(c) confirm the presence of oxygen in the O-FMWCNT samples.

The mechanism of plasma functionalization is very complex since the RF power, time, gas mixture composition, and pressure have a significant influence. As reported in table S2, increasing the RF power for 1 min of functionalization with $Ar/C_2H_6/O_2$ leads to lower oxygen percentage and sp^3 carbon percentage on the surface of MWCNTs. This can be explained by the formation of oxygen fragments from the C_2H_6 and oxygen mixture, which can etch away some of the coatings or scavenge a portion of the radicals formed in the plasma. At longer treatment times, a higher percentage of oxygen and sp^3 carbon is present in the samples. Furthermore, these percentages continue to increase by increasing the RF plasma power. This can be caused by different interactions between the plasma-produced active species with MWCNTs rather than with plasma polymer formed on the MWCNT surface. Nevertheless, the overall trend indicates that by increasing the treatment time, a higher percentage of oxygen is present on the MWCNT surface. It should be noted that oxygen functionalization at the highest plasma power level of 30 W for 20 min resulted in the chemical etching at the junction point of MWCNTs and SS, thus detaching the nanotubes from the surface of the SS mesh and damaging the electrode structure (data not shown). Therefore, it can be concluded that higher RF plasma power levels and longer treatment times provide more favorable conditions for the active species to react with the nanotubes or even damage them.

Similar to O-FMWCNT, the C 1s spectra from XPS analysis of N-FMWCNT samples are shown and deconvoluted in figure 3(a). The EDS mapping of the STEM images of N-FMWCNT for 10 W–10 min and 30 W–10 min are also presented in figures 3(b) and (c), which evidences the presence of both oxygen and nitrogen on the surface of the N-FMWCNT. As listed in table S2, for the functionalization time of 1 min, by increasing the RF power from 10 to 20 W, the sp^3 carbon increased from 9.8% to 21.2%, and then decreased to 1.4% at a RF plasma power of 30 W. This can be caused by the activation of more OH radicals at higher power levels, which can etch away the groups formed on the MWCNTs. However, at the treatment time of 10 min, the sp^3 carbon content is not affected by the increase of RF plasma power. Overall, the results reported in table S2 demonstrate that the total amount of oxygen and nitrogen groups increased significantly by increasing the functionalization time from 1 to 10 min. It should be noted that oxygen functional groups are added to N-FMWCNTs either by interacting with the plasma-produced OH radicals (detected by OES, figure S3) or through reactions between the fresh sample and atmospheric air, referred to as ageing [23, 29–31].

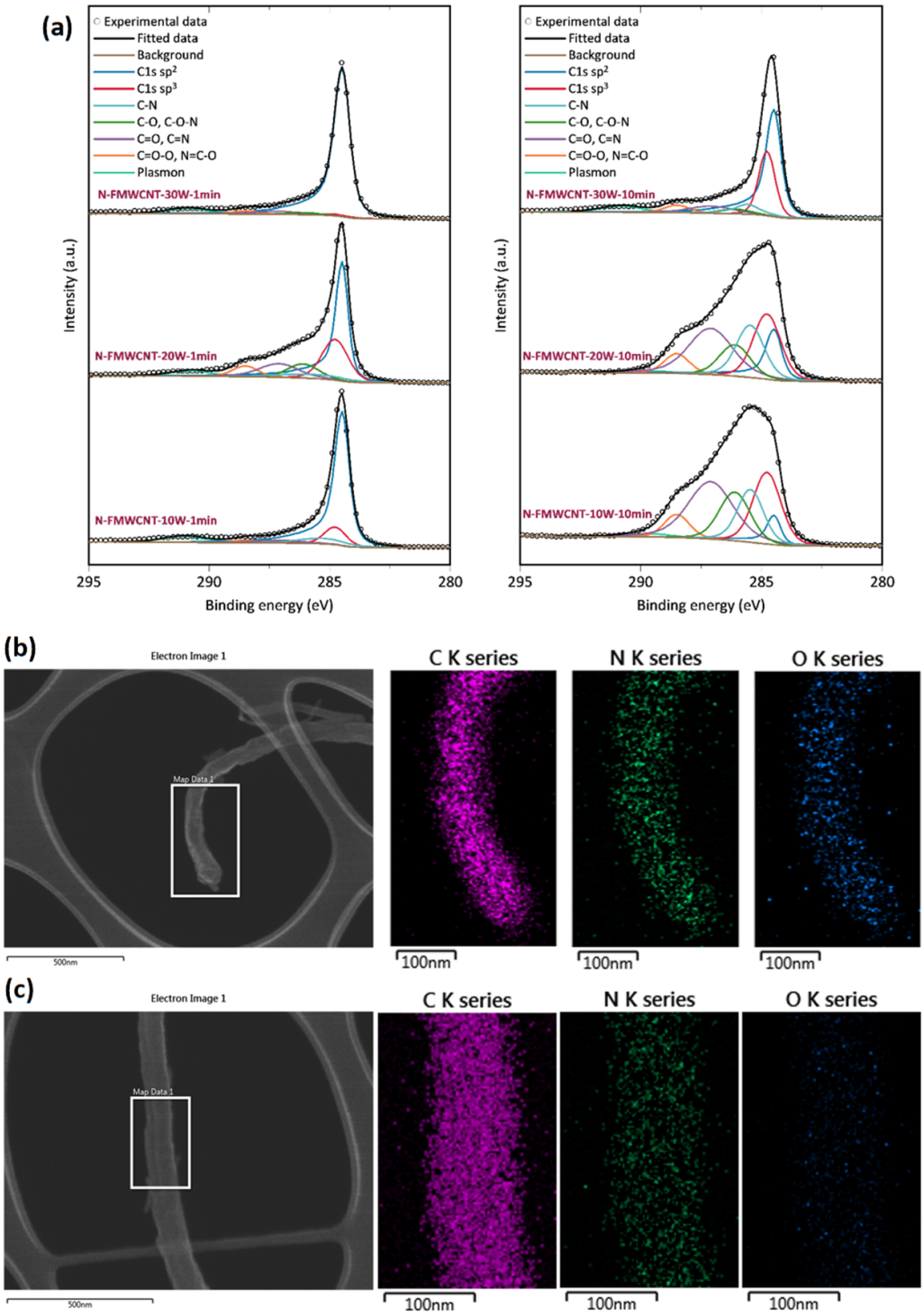

Figure 3. (a) Deconvoluted XPS spectra of C 1s for N-FMWCNT. STEM image and EDS mapping of N-FMWCNT (b) 10 W–10 min and (c) 30 W–10 min.

3.3. Electrochemical tests

Figure 4(a) shows cyclic voltammograms of MWCNTs before and after RF plasma functionalization, recorded at a scan rate of 25 mV s^{-1}. The CV recorded with the non-functionalized MWCNT shows a relatively featureless shape (on the scale of the graph presented). However, the CVs recorded with the oxygen- and nitrogen-functionalized electrodes display the shape that indicates the occurrence of redox reactions, i.e. the pseudo-capacitive behavior of the electrodes. This is evident from the presence of broad anodic and cathodic shoulders negative of −0.2 V and positive of −0.1 V. However, these redox shoulders are not well-defined due to a small percentage of functional groups added to the surface and the faster charging kinetics of the electrochemical double layer compared to the slower redox kinetics of surface functional groups [32].

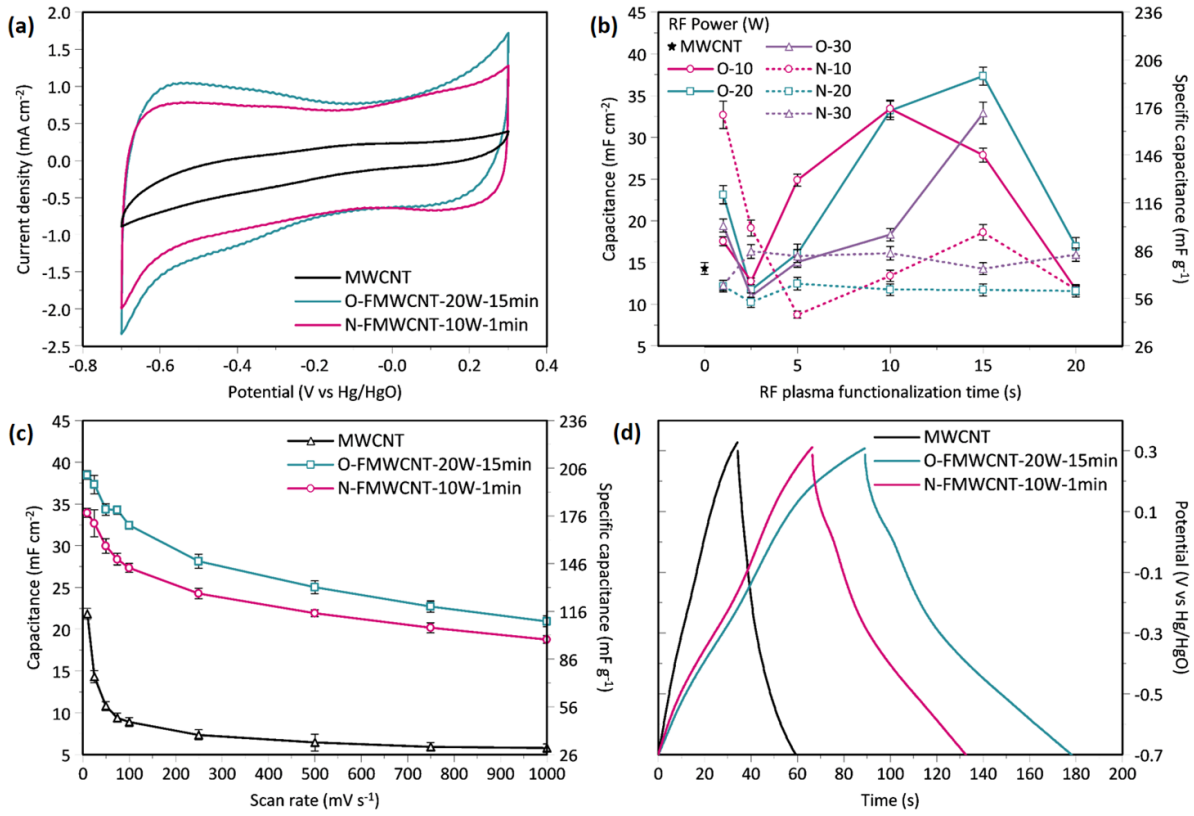

Figure 4. (a) Cyclic voltammograms of non-functionalized and functionalized MWCNTs recorded in 4 M KOH at a scan rate of 25 mV s^{-1}. (b) Capacitance of all the investigated MWCNT-based electrodes as a function of RF plasma power levels and treatment times, calculated from CVs recorded at 25 mV s^{-1}. (c) Dependence of capacitance on scan rate. (d) GCD of non-functionalized and functionalized MWCNTs recorded in 4 M KOH at the current density of 1.0 mA cm^{-2}.

The charge (area) under the O-FMWCNT and N-FMWCNT voltammograms is significantly larger than that of the bare MWCNTs, indicating an increased charge storage/delivery (i.e. capacitance). The corresponding capacitance of the electrodes was calculated using equation (1) at a scan rate of 25 mV s^{-1}, and the values are presented in figure 4(b). The results demonstrate that nitrogen and oxygen functionalities can indeed enhance the charge storage/delivery properties of the nanotubes. The O-FMWCNT electrode functionalized at a RF plasma power of 20 W for 15 min showed the highest capacitance of 37.3 ± 1.1 mF cm^{-2} (196.3 ± 5.8 F g^{-1}), and the N-FMWCNT electrode functionalized at a RF plasma power of 10 W for 2.5 min yielded a capacitance of 32.6 ± 1.6 mF cm^{-2} (171.6 ± 8.4 F g^{-1}). The capacitance of non-functionalized MWCNTs was significantly lower, 14.3 ± 0.7 mF cm^{-2} (75.3 ± 3.7 F g^{-1}). This value is in the range of values reported in the literature for non-functionalized MWCNT electrodes, 15–50 F g^{-1} [28, 33–36]. However, higher values were also reported for functionalized CNTs; for instance, Shen *et al* prepared a film of single-walled CNTs (SWCNTs) by drying a dispersion of SWCNTs over a filter paper and further dissolving the filter paper to have a thin film over a membrane. They improved the capacitance from 32.1 F g^{-1} to 146.1 F g^{-1} with 6 h of reflux treatment with nitric acid to functionalize the CNTs with carboxylic groups [34]. Likewise, Frackowaic *et al* made electrodes in a pellet shape by pressing the mixture of MWNTs, acetylene black and polyvinylidene fluoride and using gold current collector. As a result, they enhanced the capacitance of CNTs from 15 to 90 F g^{-1} by chemical KOH activation with a KOH:C ratio of 4:1, at 800 °C [33]. Although significant improvements were observed in these studies, it should be noted that the electrodes reported in the current work were produced without incorporating a binder into the carbon structure and casting the layer onto a current collector, resulting in a good electrical conductivity and high capacitance of the electrodes. Moreover, using the rapid dry plasma functionalization technique, there is no need to use chemicals or apply high temperatures during the functionalization process.

The effect of scan rate on the capacitance of the electrodes is presented in figure 4(c). As expected, by increasing the scan rate, the capacitance decreases. This decrease can be related to the kinetics of charge-transfer compensation by ion migration. Namely, at higher scan rates, due to the presence of nano-scale pores on the MWCNTs (figure 1), the migration of ions within/inside the pores is limited, rendering the MWCNT surface area accessible for the charge storage smaller. However, it can be noted that the decrease in capacitance on the functionalized MWCNT is much smaller than that on pristine MWCNT. Thus, the capacitance of the O-FMWCNT and N-FMCNT recorded at 1000 mV s^{-1} decreased down to ca. 55% of the value recorded at 10 mV s^{-1}, while on the non-functionalized

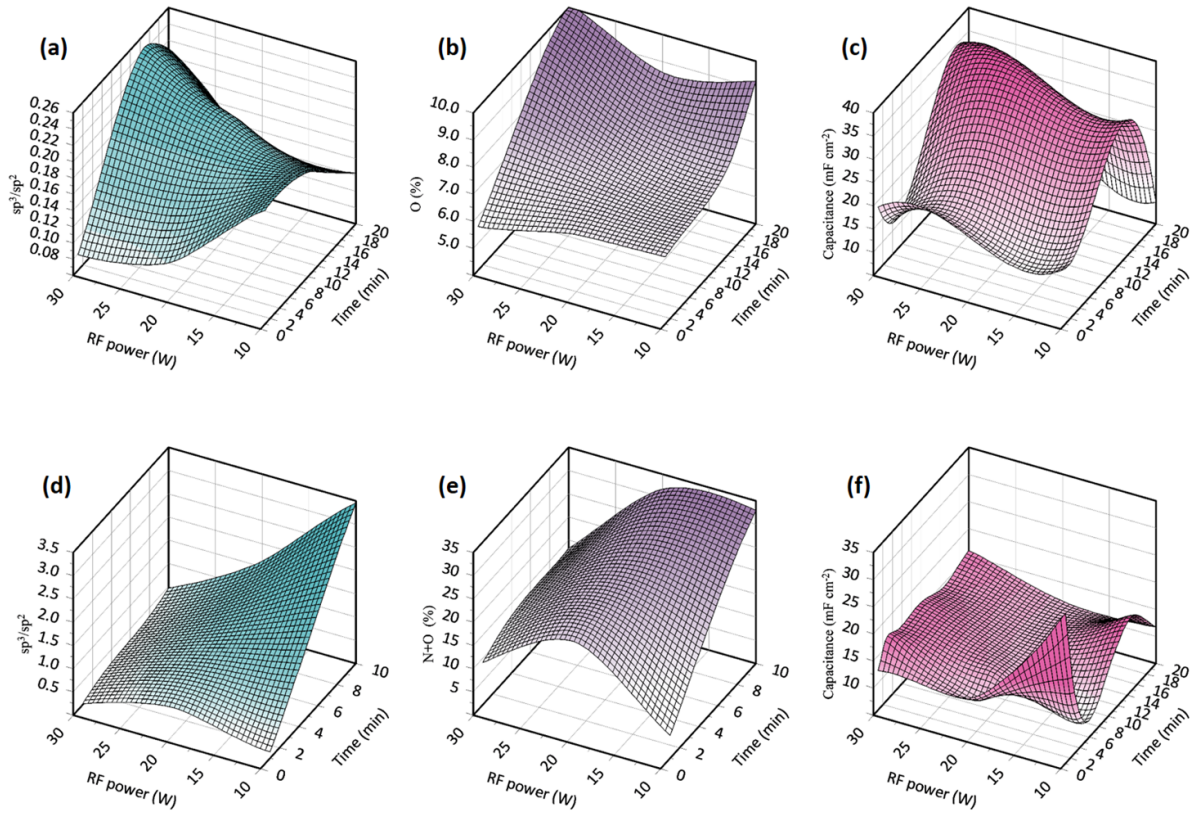

Figure 5. The influence of RF plasma power and time on the (a), (d) the sp^3 to sp^2 ratio, (b), (e) percentage of functional groups, and (c), (f) capacitance of O-FMWCNT and N-MWCNT, respectively.

MWCNT the value decreased much more, down to 26%. This indicates that the functionalized MWCNTs offer a 3D structure that is more favorable for ion migration than that one offered by the pristine MWCNT.

The GCD measurements were performed at 1.0 mA cm^{-2}, and the charge–discharge curves are provided in figure 4(d). The observed divergence from the general linear triangular form of the curves is due to the existence of redox reactions on the surface of MWCNTs, which contribute to additional charge storage. The curve recorded with the non-functionalized MWCNT also shows a slight deviation from linearity, indicating that there is also the occurrence of redox surface reactions even on this surface, to a certain degree. Figure 4(d) shows that the charge–discharge duration of the MWCNT electrode is the shortest, whereas the charge–discharge time of the N-FMWCNT and O-FMWCNT is longer, indicating larger charge storage-delivery of the latter two surfaces, similar to what is observed in voltammograms in figure 4(a) [4]. Employing equation (2), the capacitance values from the GCD curves were calculated to be 10.7 ± 0.5, 24.9 ± 1.3 and 33.8 ± 0.9 mF cm^{-2} or 56.3 ± 2.6, 131.1 ± 6.8 and 177.9 ± 4.7 F g^{-1} for the MWCNT, N-FMWCNT and O-FMWCNT electrode materials. The enhanced pseudocapacitive behavior of the F-MWCNTs, through both the occurrence of the redox reaction of the functional groups at the electrode–electrolyte interface and increased accessibility of the MWCNT surface to the electrolyte, leads to a higher capacitance of the electrodes [37].

The interpolation matrix of the effect of RF plasma power and time on the percentage of sp^3-to-sp^2 carbon ratio (calculated from the XPS results), functional groups and the corresponding capacitance are reported in the 3D plots in figure 5. Figures 5(a) and (b) illustrate that by increasing the RF plasma time at different RF plasma power level, the percentage of oxygen on the MWCNT surface increases. It seems that more reactions occur on the MWCNT surface at higher treatment time, resulting in adding more oxygen-containing groups to the MWCNT surface. The sp^3-to-sp^2 ratio in the carbon changes over a small range. Figure 5(a) shows that an increase in the RF plasma power level results in a decrease of sp^3 carbon at short functionalization times, which can be due to the removal of amorphous carbon from the MWCNTs by the strong oxygen active species. At longer functionalization times (ca. 10–15 min) and higher RF plasma powers, the sp^3-to-sp^2 carbon ratio increases as a consequence of the addition of more oxygen-containing groups to the surface. However, at higher RF powers and times past 15 min, the sp^3-to-sp^2 carbon ratio decreases, which can be explained by the structural damage caused by active oxygen species and consequential chemical etching at the junction point of MWCNTs and SS, resulting in detachment of the nanotubes. On the other hand, figure S4 displaying the Raman spectra (normalized to G band) of all functionalized samples under different RF plasma functionalization conditions indicates that the *R*-value (I_D/I_G ratio) is sensitive to surface modifications upon plasma treatment. As the RF plasma power and time increase, the

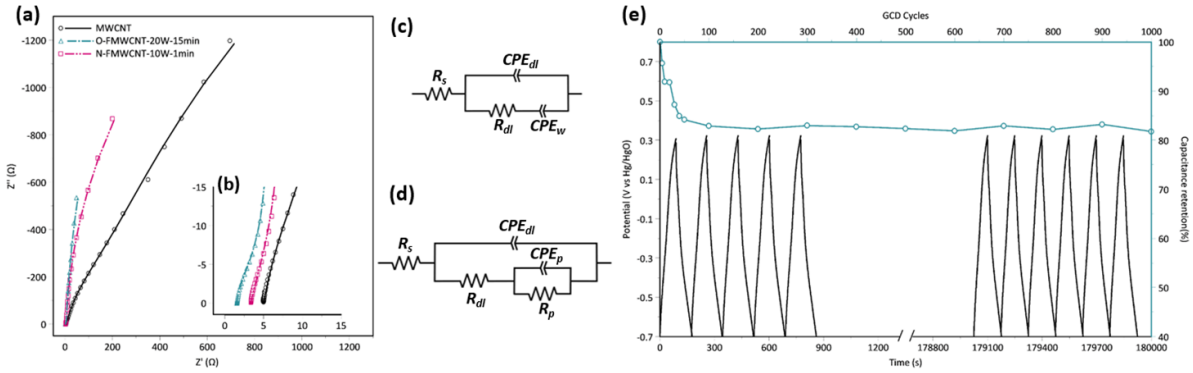

Figure 6. (a) Nyquist plots of MWCNT before and after plasma functionalization (inset: (b) low-frequency region), (c) and (d) the equivalent circuits, and (e) GCD stability of O-FMWCNT for 1000 cycles at a current density of 1 mA cm^{-2}.

intensity of the D band and consequently the R-value increase, corresponding to the presence of more structural defects in the nanotubes, which can be originated from the reduced π-conjugated states (figures S4(a)–(c)) [38]. A similar trend is observed for the capacitance of the electrodes. The capacitance of the O-FMWCNT electrodes (figure 5(c)) increases by applying higher RF plasma power levels and longer functionalization time, which resulted from the addition of more oxygen-containing groups and a higher sp^3-to-sp^2 carbon ratio on the surface of MWCNTs. However, as mentioned earlier, at high RF plasma time and power, the occurrence of chemical etching can reduce the surface area of the electrode by detaching the nanotubes from the SS, resulting in a substantial decrease in capacitance, as evidenced in figure 5(c).

Increasing the RF plasma treatment time with the nitrogen-containing gas mixture leads to a more substantial increase of the number of functional groups and sp^3 carbon on the surface of MWCNTs, compared with oxygen (figure 5). However, with an increase in RF plasma power levels at shorter times, the corresponding values first increase and then drop (figures 5(a) and (b)). The corresponding Raman spectra (figures S4(d)–(f)) demonstrate a decrease in the intensity of the D band, followed by an increase. It has been reported that different competing mechanisms take place during plasma functionalization; etching or removal of surface defects/amorphous carbons by plasma active species, deposition of plasma polymer on the surface, and addition of functional groups to the surface [19, 39]. It appears that at low power levels, the excited species produced in the nitrogen-containing plasma can remove the amorphous carbon from the MWCNTs and lower the sp^3-to-sp^2 carbon ratios in their structure. This result is confirmed by the appearance of a less intense D band in the Raman spectra shown in figures S4(d)–(f), leading to a lower R (I_D/I_G) value associated with MWCNTs with fewer structural defects. However, at higher plasma power levels, the active species can functionalize or form an amorphous layer over the graphitic layers of MWCNTs. At higher RF plasma power levels, more collision between the plasma-produced active species can reduce their energy level, which will not be sufficient for etching away the incorporated functional groups or the deposited amorphous carbon [19, 39, 40]. However, at higher RF plasma power levels and longer functionalization times, a more significant broadening of the D and G bands is observed as illustrated in figures S4(d)–(f). This is associated with more structural defects, similarly to the MWCNTs synthesized at low temperature (figure S1(f)). Figure 5(f) shows that the capacitance of the N-FMWCNT electrodes seems to be relatively independent of the plasma conditions and surface chemistry. This can be attributed to the existence of a much higher sp^3-to-sp^2 carbon ratio (figure 5(d)) than O-FMWCNT electrodes (figure 5(a)), which damages the structural integrity of MWCNTs, further affecting their electrochemical performance.

The impedance behavior of the electrodes was assessed using EIS, and the Nyquist plots of MWCNTs before and after functionalization are reported in figure 6(a). It is evident from the quasi-linear/vertical shape of the Nyquist plots that the capacitive contribution dominates the impedance behavior. Unlike pure electrical double-layer capacitors that show a vertical line, the frequency dependence of the real impedance component reveals the pseudo-capacitive properties and/or the existence of impedance resulting from the porosity of all three electrodes. A slightly sloped and curved line in the lower frequency region and a semicircle-like behavior in the higher frequency region (figure 6(b)) originate from the kinetics of the redox reaction and ion movement inside the pores, contributing to the actual impedance component, thus yielding two time constants [41].

The impedance behavior of the electrodes was modeled using the equivalent electrical circuits (EEC) presented in figures 6(c) and (d); the response of the non-functionalize MWCNT electrode was modeled by the EEC in figure 6(c), while the response of the two functionalized electrodes was modeled using the EEC in figure 6(d). In these EECs, R_s, represents the electrolyte resistance, the internal electrode material resistance, and contact resistance between MWCNT and the SS mesh (current collector). The capacitance related to the electrostatic charging of the double-layer (CPE_{dl}) and the resistance for ion migration to compensate the charge (R_{dl}) is described through the CPE_{dl}-R_{dl} time constant, corresponding to the response of the system in the higher-frequency region. The CPE_W element in figure 6(c) represents the impedance related to the migration of ions through the pores of the MWCNT electrode during the charging/discharging process.

For the two functionalized electrodes, their pseudo-capacitive behavior can be characterized through the pseudo-capacitance (CPE_p) and its corresponding polarization resistance (R_p), representing the lower-frequency range CPE_p-R_p time constant. Due to the presence of surface roughness, porosity, surface inhomogeneity and non-uniform charge distribution, a constant-phase-element (CPE) was used instead of a pure capacitance [42–45]. Table S3 reports the values of the equivalent circuit components. The values of CPE_{dl} power, n_{dl}, deviate from the value for pure capacitance ($n = 1$), which could be due to the heterogeneity (in terms of the surface-charge distribution and morphology) of the MWCNTs. It can be seen that the CPE_{dl} value increases after functionalization of the MWCNT, while the corresponding R_{dl} value decreases, which can be due to the enhancement of surface wettability, offering a more accessible surface area of MWCNT to the electrolyte. Table S3 shows that the pseudo-capacitance (CPE_p) of the O-FMWCNT is higher than that of the N-FMWCNT, which agrees with the CV and GCD results presented earlier in the text. However, it can be noticed that the R_p value for the O-FMWCNT is higher than that recorded for the N-FMWCNT electrode, indicating a slower kinetics of surface redox reactions. This, in turn, indicates that the increased capacitance of the O-FMWCNT surface recorded by CV, GCD, and CPE values in EIS, can also be due to the increased accessibility of the O-FMWCNT surface to the electrolyte, in addition to the contribution of the surface-redox reactions to the total charge storage/delivery capacitance.

The charge–discharge cyclability of the O-FMWCNT-20 W–15 min electrode was tested by performing GCD for 1000 cycles at a current density of 1 mA cm^{-2}. The results in figure 6(b) show 82% retention of the initial capacitance of the electrodes after 1000 cycles. However, the capacitance increased to its initial value after equilibrating the electrode at the open circuit and repeating the experiment (data not shown). Thus, this drop in capacitance with cycling can be attributed to the drying of the MWCNTs' deep pores, resulting in a lower surface area and thus, a lower capacitance. McArthur *et al* [28] and Frackowiak *et al* [46] observed a similar phenomenon and explained the reversibility of this reduction after allowing the electrode to equilibrate at an open circuit.

4. Conclusion

MWCNTs with a forest-like structure were directly grown on SS meshes without the use of any catalyst to produce binder-free electrodes that were tested for application in SCs. We demonstrated that the RF capacitively-coupled plasma can be used as a dry MWCNT functionalization method to improve the electrode's charge storage/delivery performance. The porous MWCNT-SS electrode's surface was further modified by using different gas mixtures at different RF plasma power levels and treatment times in order to functionalize the MWCNT surface with oxygen and nitrogen functional groups. It was illustrated that processing parameters, including plasma power and time, indeed governed the surface chemistry of the functionalized nanotubes and thus their capacitive behavior. The capacitance of the MWCNTs electrodes increased from 75.3 ± 3.7 F g^{-1} to 196.3 ± 5.8 F g^{-1} after functionalization by RF plasma using an $Ar/C_2H_6/O_2$ gas mixture at 20 W for 15 min, without any damage to the structure of the MWCNTs. Accordingly, the solvent-free RF plasma method provides convenient and mild operating conditions to ensure the functionalization of carbon-based material used for various applications.

Data availability statement

All data that support the findings of this study are included within the article (and any supplementary files).

Acknowledgments

The authors acknowledge the financial support of the Faculty of Engineering through the McGill Engineering Doctoral Award (MEDA), the Natural Sciences and Engineering Research Council of Canada (NSERC), the Gerald Hatch Faculty Fellowship, and the Fonds de Recherche du Québec—Nature et technologies (FRQNT). The authors thank the technical staff of the Department of Chemical Engineering at McGill University for their assistance. The authors acknowledge Dr Boris Nijikovsky for the TEM work.

Conflict of interest

There are no conflicts to declare.

ORCID iDs

Elmira Pajootan https://orcid.org/0000-0002-6869-3689
Sylvain Coulombe https://orcid.org/0000-0001-9521-181X

References

[1] Davies A and Yu A 2011 Material advancements in supercapacitors: from activated carbon to carbon nanotube and graphene *J. Neurosci. Res.* **89** 1342–57
[2] Dou S *et al* 2018 Plasma-assisted synthesis and surface modification of electrode materials for renewable energy *Adv. Mater.* **30** 1705850
[3] Goodenough J B 2014 Electrochemical energy storage in a sustainable modern society *Energy Environ. Sci.* **7** 14–18
[4] Wu X, Yang H, Yu M, Liu J and Li S 2021 Design principles of high-voltage aqueous supercapacitors *Mater. Today Energy* **21** 100739
[5] Movassagh-Alanagh F, Bordbar-Khiabani A and Ahangari-Asl A 2019 Fabrication of a ternary PANI@Fe_3O_4@CFs nanocomposite as a high performance electrode for solid-state supercapacitors *Int. J. Hydrog. Energy* **44** 26794–806
[6] Sridhar D, Yu H, Meunier J-L and Omanovic S 2020 Carbon nano-fiber forest foundation for ruthenium oxide pseudo-electrochemical capacitors *Mater. Adv.* **1** 215–27

[7] Xie P, Yuan W, Liu X, Peng Y, Yin Y, Li Y and Wu Z 2021 Advanced carbon nanomaterials for state-of-the-art flexible supercapacitors *Energy Storage Mater.* **36** 56–76

[8] Wang Y, Wu X, Han Y and Li T 2021 Flexible supercapacitor: overview and outlooks *J. Energy Storage* **42** 103053

[9] Pajootan E, Omanovic S and Coulombe S 2021 Controllable dry synthesis of binder-free nanostructured platinum electrocatalysts supported on multi-walled carbon nanotubes and their performance in the oxygen reduction reaction *Chem. Eng. J.* **426** 131706

[10] Pajootan E, Coulombe S and Omanovic S 2021 Two-step dry synthesis of binderless 3D low Pt-loading electrocatalysts for direct alkaline methanol fuel cell anodes *ACS Appl. Energy Mater.* **4** 11514–27

[11] Sridhar D, Meunier J-L and Omanovic S 2019 Directly grown carbon nano-fibers on nickel foam as binder-free long-lasting supercapacitor electrodes *Mater. Chem. Phys.* **223** 434–40

[12] Ilnicka A, Skorupska M, Szkoda M, Zarach Z, Kamedulski P, Zielinski W and Lukaszewicz J P 2021 Combined effect of nitrogen-doped functional groups and porosity of porous carbons on electrochemical performance of supercapacitors *Sci. Rep.* **11** 18387

[13] Meng L, Fu C and Lu Q 2009 Advanced technology for functionalization of carbon nanotubes *Prog. Nat. Sci.* **19** 801–10

[14] Eskandarian L, Arami M and Pajootan E 2014 Evaluation of adsorption characteristics of multiwalled carbon nanotubes modified by a poly(propylene imine) dendrimer in single and multiple dye solutions: isotherms, kinetics, and thermodynamics *J. Chem. Eng. Data* **59** 444–54

[15] Mallakpour S and Soltanian S 2016 Surface functionalization of carbon nanotubes: fabrication and applications *RSC Adv.* **6** 109916–35

[16] Corella Puertas E, Peyot M-L, Pineda M, Volk K, Coulombe S and Yargeau V 2021 Degradation of diatrizoate in a pin-to-liquid plasma reactor, its transformation products and their residual toxicity *Sci. Total Environ.* **782** 146895

[17] Martin-del-campo J, Uceda M, Coulombe S and Kopyscinski J 2021 Plasma-catalytic dry reforming of methane over Ni-supported catalysts in a rotating gliding arc—spouted bed reactor *J. CO_2 Util.* **46** 101474

[18] Saka C 2018 Overview on the surface functionalization mechanism and determination of surface functional groups of plasma treated carbon nanotubes *Crit. Rev. Anal. Chem.* **48** 1–14

[19] Nair L G, Mahapatra A S, Gomathi N, Joseph K, Neogi S and Nair C P R 2015 Radio frequency plasma mediated dry functionalization of multiwall carbon nanotube *Appl. Surf. Sci.* **340** 64–71

[20] Xu T, Yang J, Liu J and Fu Q 2007 Surface modification of multi-walled carbon nanotubes by O_2 plasma *Appl. Surf. Sci.* **253** 8945–51

[21] Vesel A and Mozetic M 2017 New developments in surface functionalization of polymers using controlled plasma treatments *J. Phys. D: Appl. Phys.* **50** 293001

[22] Meyyappan M 2011 Plasma nanotechnology: past, present and future *J. Phys. D: Appl. Phys.* **44** 174002

[23] Jorge L, Coulombe S and Girard-Lauriault P-L 2015 Nanofluids containing MWCNTs coated with nitrogen-rich plasma polymer films for CO_2 absorption in aqueous medium *Expert Opin. Drug Deliv.* **12** 1311–21

[24] Hussain S, Amade R, Jover E and Bertran E 2013 Nitrogen plasma functionalization of carbon nanotubes for supercapacitor applications *J. Mater. Sci.* **48** 7620–8

[25] Roy A, Ray A, Saha S, Ghosh M, Das T, Satpati B, Nandi M and Das S 2018 NiO-CNT composite for high performance supercapacitor electrode and oxygen evolution reaction *Electrochim. Acta* **283** 327–37

[26] Ramya S, Anita T, Shaikh H and Dayal R K 2010 Laser Raman microscopic studies of passive films formed on type 316LN stainless steels during pitting in chloride solution *Corros. Sci.* **52** 2114–21

[27] Chen J, Xiao Q, Lu Z, Ru X, Peng H, Xiong Q and Li H 2017 Characterization of interfacial reactions and oxide films on 316L stainless steel in various simulated PWR primary water environments *J. Nucl. Mater.* **489** 137–49

[28] McArthur M A, Hordy N, Coulombe S and Omanovic S 2015 A binder-free multi-walled carbon nanotube electrode containing oxygen functionalities for electrochemical capacitors *Electrochim. Acta* **162** 245–53

[29] Jorge L, Girard-Lauriault P-L and Coulombe S 2017 pH-reversible destabilization-dispersion of MWCNTs coated with functional plasma polymer films in water *Plasma Process. Polymers* **14** 1700026

[30] Hordy N, Coulombe S and Meunier J-L 2013 Plasma functionalization of carbon nanotubes for the synthesis of stable aqueous nanofluids and poly(vinyl alcohol) nanocomposites *Plasma Process. Polymers* **10** 110–8

[31] Stancu E C, Stanciuc A-M, Vizireanu S, Luculescu C, Moldovan L, Achour A and Dinescu G 2014 Plasma functionalization of carbon nanowalls and its effect on attachment of fibroblast-like cells *J. Phys. D: Appl. Phys.* **47** 265203

[32] Choi C, Kim K M, Kim K J, Lepró X, Spinks G M, Baughman R H and Kim S J 2016 Improvement of system capacitance via weavable superelastic biscrolled yarn supercapacitors *Nat. Commun.* **7** 13811

[33] Frackowiak E, Jurewicz K, Szostak K, Delpeux S and Béguin F 2002 Nanotubular materials as electrodes for supercapacitors *Fuel Process. Technol.* **77–78** 213–9

[34] Shen J, Liu A, Tu Y, Foo G, Yeo C, Chan-Park M B, Jiang R and Chen Y 2011 How carboxylic groups improve the performance of single-walled carbon nanotube electrochemical capacitors? *Energy Environ. Sci.* **4** 4220–9

[35] Li X, Gu T and Wei B 2012 Dynamic and galvanic stability of stretchable supercapacitors *Nano Lett.* **12** 6366–71

[36] Pan H, Li J and Feng Y 2010 Carbon nanotubes for supercapacitor *Nanoscale Res. Lett.* **5** 654

[37] Chauhan N P S, Mozafari M, Chundawat N S, Meghwal K, Ameta R and Ameta S C 2016 High-performance supercapacitors based on polyaniline–graphene nanocomposites: some approaches, challenges and opportunities *J. Ind. Eng. Chem.* **36** 13–29

[38] Abdel-Fattah E, Ogawa D and Nakamura K 2017 Oxygen functionalization of MWCNTs in RF-dielectric barrier discharge Ar/O_2 plasma *J. Phys. D: Appl. Phys.* **50** 265301

[39] Daletou M K and Aggelopoulos C A 2021 Highly-energy efficient oxidation of MWCNT with nanosecond pulsed dielectric barrier discharge plasma *Appl. Surf. Sci.* **563** 150139

[40] Saikia N J, Ewels C, Colomer J-F, Aleman B, Amati M, Gregoratti L, Hemberg A, Thiry D, Snyders R and Bittencourt C 2013 Plasma fluorination of vertically aligned carbon nanotubes *J. Phys. Chem.* C **117** 14635–41

[41] Yu H, Sridhar D and Omanovic S 2021 Ru_xBi_{1-x}-oxide as an electrode material for pseudocapacitors *Can. J. Chem. Eng.* (https://doi.org/10.1002/cjce.24306)
[42] Pajootan E and Arami M 2013 Structural and electrochemical characterization of carbon electrode modified by multi-walled carbon nanotubes and surfactant *Electrochim. Acta* **112** 505–14
[43] Mei B-A, Munteshari O, Lau J, Dunn B and Pilon L 2018 Physical interpretations of Nyquist plots for EDLC electrodes and devices *J. Phys. Chem.* C **122** 194–206
[44] Simon P and Gogotsi Y 2008 Materials for electrochemical capacitors *Nat. Mater.* **7** 845–54
[45] Bathula C, Rabani I, Kadam A, Opoku H, Patil S A, Shreshta N K, Hwang J-H, Seo Y-S and Kim H-S 2022 Sonochemically exfoliated polymer-carbon nanotube interface for high performance supercapacitors *J. Colloid Interface Sci.* **606** 1792–9
[46] Frackowiak E, Jurewicz K, Delpeux S and Béguin F 2001 Nanotubular materials for supercapacitors *J. Power Sources* **97–98** 822–5